JOURNAL OF MATERIALS SCIENCE 24 (1989) 3855–3864

Dual-phase magnesia–zirconia ceramics with strength retention at elevated temperatures

THOMAS C. YUAN, G. V. SRINIVASAN, JAN FONG JUE, ANIL V. VIRKAR
Department of Materials Science and Engineering, University of Utah, Salt Lake City, Utah 84112, USA

Two-phase polycrystalline ceramics containing MgO and ZrO_2 were fabricated by pressureless sintering powder compacts in air to near theoretical density. MnO was added as a densification aid in most compositions. For samples fabricated with 20 vol% ZrO_2 and 80 vol% MgO (which actually contained ~23 vol% ZrO_2(ss) after sintering because some of the MgO dissolved in zirconia), densities in excess of 98% theoretical were achieved at temperatures as low as about 1250° C. However, most of the samples were typically sintered at 1420 ± 10° C. The grain sizes of the two phases, ZrO_2(ss) and MgO(ss), were of the order of 1.4 μm. Thermal etching of the specimens showed the presence of very uniform sized domains (approximately 240 nm in size) in zirconia grains. Some samples were also fabricated in which 8 mol% CaO was added in order to stabilize the high-temperature cubic polymorph of zirconia to room temperature. The grain sizes of the two phases in this composition were also of the order of 1.4 μm. No domains were observed in zirconia grains in CaO-doped samples. Fracture strength was measured as a function of volume fraction of zirconia. Strength values in excess of 500 MPa have been measured on samples fabricated with 40 vol% zirconia (the amount of zirconia(ss) is ~43 vol%). Samples of similar composition but with CaO doping exhibited strength of the order of 300 MPa despite an essentially identical grain size and density. Fracture toughness of samples containing CaO was 3.0 MPa $m^{1/2}$ while that of the samples without CaO was 5.2 MPa $m^{1/2}$. No monoclinic phase was observed on either the fracture or the ground surfaces of CaO-doped and undoped samples. Fracture strength and toughness, measured as a function of temperature up to 1000° C, were found to be nearly independent of temperature. The temperature independence of the strength suggests that strengthening and toughening in this material does not occur by transformation toughening.

1. Introduction

Considerable work on MgO-partially stabilized zirconia has shown that high strength and toughness in this system can be realized by careful processing and thermal treatment procedures [1–7]. The dominant toughening mechanism in this material, nominally doped with 8 to 11 mol% MgO, has been identified to be transformation toughening. A typical fabrication procedure consists of sintering powder compacts of appropriate compositions in the stability range of the cubic phase field followed by an ageing treatment at a lower temperature. The ageing treatment is carried out either just above the eutectoid temperature (at ~1420° C) wherein proeutectoid tetragonal phase precipitates out of the supersaturated cubic phase [2, 7], or a subeutectoid treatment in which samples are annealed at ~1100° C [4].

Toughening of many ceramic matrices such as alumina [8], mullite [9], β''-alumina [10], Si_3N_4 [11] etc. has been accomplished by the incorporation of metastable tetragonal zirconia particles as dispersants. Most of the work in the MgO–ZrO_2 system, however, has been done on compositions containing zirconia as the major constituent with magnesia added as a stabilizer. An examination of the MgO–ZrO_2 pseudobinary phase diagram [12–14] indicates that the CaF_2-type solid solution decomposes eutectoidally into tetragonal zirconia and MgO, saturated with ZrO_2 at about 1400° C. This suggests the possibility of strengthening MgO matrix ceramics dispersed with tetragonal zirconia. Other than the work of Ikuma *et al.* [15], no work has been reported in the literature on toughening of magnesia with dispersed zirconia phase. From a practical point of view, toughened MgO may have potential applications because its thermal expansion coefficient is rather high. Thus, in applications requiring matching of thermal expansion characteristics with other structural materials, cast iron in particular, MgO may be an ideal material if it can be strengthened and if its thermal shock characteristics can be improved. This study was undertaken with the specific objective of improving mechanical properties of MgO matrix ceramics by the incorporation of zirconia.

Fabrication of MgO–ZrO_2 two-phase ceramics in the present study was achieved by pressureless sintering isostatically pressed powder compacts as well as slip-cast specimens. Densification was facilitated by the addition of MnO, and in some cases FeO, as a sintering

0022–2461/89 $03.00 + .12

aid. Some of the samples were also fabricated with CaO as a dopant used for stabilizing the cubic phase of zirconia to room temperature. Strength and toughness were measured as a function of temperature from room temperature to 1000° C. Samples were examined by X-ray diffraction for phase identification. Microstructural characterization, which included the determination of the volume fractions of the two phases and the measurement of the grain sizes, was done using optical microscopy and scanning electron microscopy. The experimental procedure, results and discussion of the results are presented in the following sections.

2. Experimental procedure

2.1. Sample fabrication

2.1.1. Powder preparation and green forming

MgO (Dow Chemical Co., Midland, Michigan, and Fisher Scientific, Fair Lawn, New Jersey) and ZrO_2 (Dow Chemical Co., Midland, Michigan, and Daichi DK-1 Zirconia Sales (America), Atlanta, Georgia) powders from commercial sources were used in the present study. The typical particle size of MgO and ZrO_2 powders was of the order of 0.5 to 1 μm. Two methods of green forming was employed in the present work: isostatic pressing and slip casting. For isostatic pressing, MgO was dispersed in an aqueous medium containing 2% NH_4OH at a pH of $\approx$11. Prior studies showed that dispersion of MgO occurred readily at a pH of 11 [16]. $Mn(NO_3)_2$ used as a source of MgO, was dissolved in the slurry. In some cases, FeO powder was added as a dopant. The rationale for manganese or iron addition will be discussed later. In some mixtures, CaO was added in order to stabilize the cubic polymorph of zirconia to room temperature. The powder was milled for 12 h, dried in an oven for 4 h at 250° C and then calcined at 1000° C for 4 h in air in an alumina crucible. The powder was then dispersed in cyclohexane and the requisite amount of ZrO_2 was added to it. The mixture was vibratory milled for 12 h, pan dried and passed through a 100 mesh screen. Bars and pellets were green formed by die-pressing under a pressure of 30 MPa followed by isostatic pressing at 200 MPa.

For slip casting, MgO and ZrO_2 powders were dispersed in an aqueous medium containing 2% NH_4OH. $Mn(NO_3)_2$ as a dopant was added to the mixture. The powder mixture was milled for 12 h, dried in an oven at 250° C for 4 h followed by a calcination step at 1000° C for 4 h. The powder was dry ground and passed through a 100 mesh screen. Subsequently, a slurry was formed in ethyl alcohol with 0.5 wt % PVB as a binder. The mixture was vibratory milled for 12 h and the resulting slip was poured into a plaster of paris mould. The samples, typically in the shape of a crucible or a plate, were released after 12 h, and dried in air for 24 h. Samples were subsequently bisque fired at 1000° C in air for 1 h.

2.1.2. Sintering

Samples were sintered in air for 2 h over a range of temperatures from 1000 to 1500° C. In manganese-doped samples, densities in excess of 97% theoretical were achieved at temperatures as low as 1250° C. Typically, however, the samples were sintered at 1420 $\pm$ 10° C for 2 h. After sintering, the samples were furnace-cooled to room temperature. Some of the samples were subsequently annealed at 1650° C for up to 120 h in order to examine the grain growth characteristics.

2.2. Mechanical characterization

Mechanical characterization consisted of the measurement of strength and toughness as a function of temperature. Typical sample dimensions of the strength bars was 4.5 mm $\times$ 4.5 mm $\times$ 45 mm. Strength was measured in four-point bending with inner span = 20.0 mm and outer span = 40.0 mm. The loading rate was 0.127 mm min^{-1}. Strength was measured as a function of temperature from room temperature to 1000° C. Fracture toughness, K_c, was measured using single-edge notched beam (SENB) specimens in three-point bending with span equal to 30 mm. Typical sample dimensions were 4.5 mm $\times$ 9.5 mm $\times$ 35 mm. Notches were machined using a diamond blade $\sim$150 μm thick. K_c was also measured as a function of temperature up to 1000° C.

2.3. Microstructural characterization and phase identification

Samples were characterized with regards to density, microstructure, and phase content. Density was measured by a conventional fluid immersion method. For microstructural evaluation, samples were metallographically polished. No etching was necessary to reveal the different phases as the contrast between the zirconia- and magnesia-rich regions was large. Volume fractions of the magnesia- and zirconia-rich phases were determined by systematic point-counting procedure. However, samples were thermally etched in order to reveal the fine structure (discussed in Section 3) within the zirconia-rich regions. The grain size was measured using the linear intercept method. As-sintered, ground and fracture surfaces were examined by X-ray diffraction using Cu$K\alpha$ radiation. The objectives were to identify the various phases and to determine if the monoclinic phase could be detected in the as-sintered, ground or fracture surfaces. Fractured samples were also examined under an optical and a scanning electron microscope in order to identify the fracture origin and the strength-limiting flaw.

3. Results

3.1. Sample fabrication and microstructural characterization

Figs 1 to 3 show densities of sintered samples as a function of temperature for various compositions. For the estimation of densities of the sintered samples in terms of per cent theoretical, the theoretical densities of MgO(ss) and ZrO_2(ss) were assumed to be 3.58 and 5.8 g ml^{-1}, respectively. All the samples were sintered for 2 h in air. Fig. 1 shows relative density (% theoretical) as a function of sintering temperature from 1000 to 1500° C for pure MgO and 80 vol % MgO–20 vol % ZrO_2 samples. (All compositions are given on the basis of starting mixtures. Volume fractions of

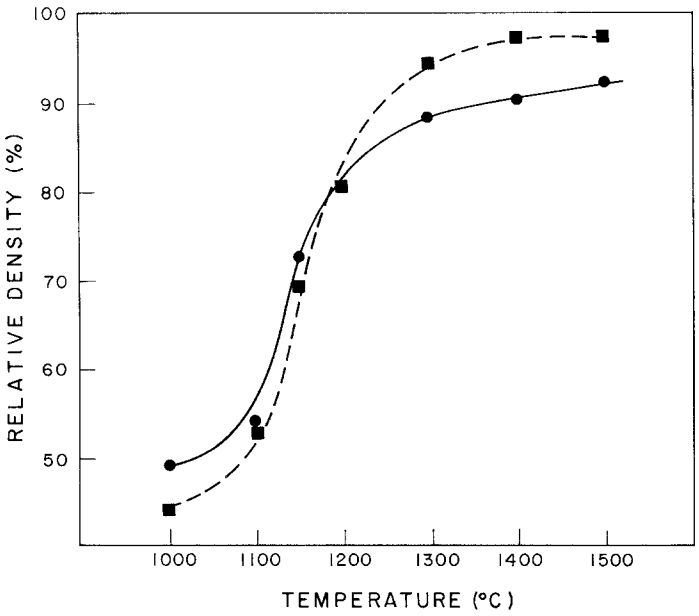

Figure 1 The effect of temperature on percent theoretical density of (●) pure MgO (Fisher) and (■) MgO + 20 vol % ZrO_2 (Daiichi) samples sintered for 2 h in air.

the two phases were measured on samples made with ZrO_2 content between 10 and 60 vol % on the basis of starting compositions. A systematic point-counting procedure was employed for the determination of the volume fractions. These data are given in Table I.) Below 1200° C, the presence of zirconia was found to hinder densification while above 1200° C, samples containing ZrO_2 densified to a higher end point density. Fig. 2a shows the effect of MnO as a dopant on the relative density for 80 vol % MgO–20 vol % ZrO_2. As seen in the figure, the densification is considerably more rapid with MnO additions as compared to the

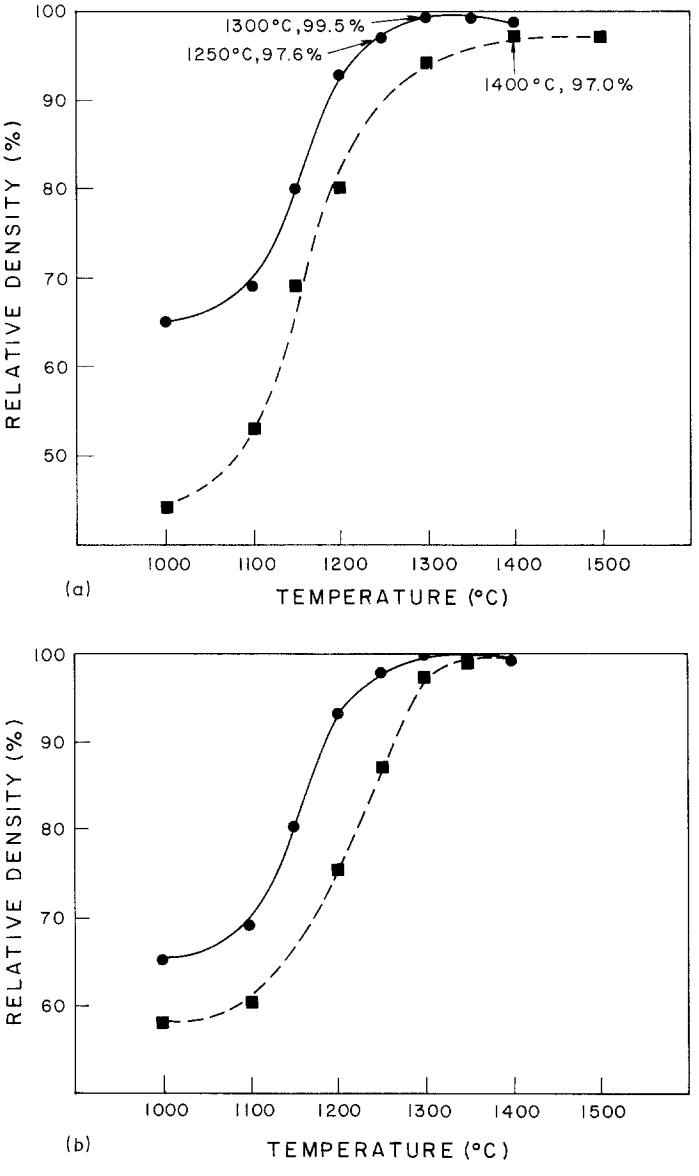

Figure 2 (a) Per cent theoretical density of MgO + 20 vol % ZrO_2 (●) with and (■) without 2% MnO. (b) The effect of the concentration of MnO on end-point density of MgO + 20 vol % ZrO_2: (●) 2% MnO, (■) 3% MnO.

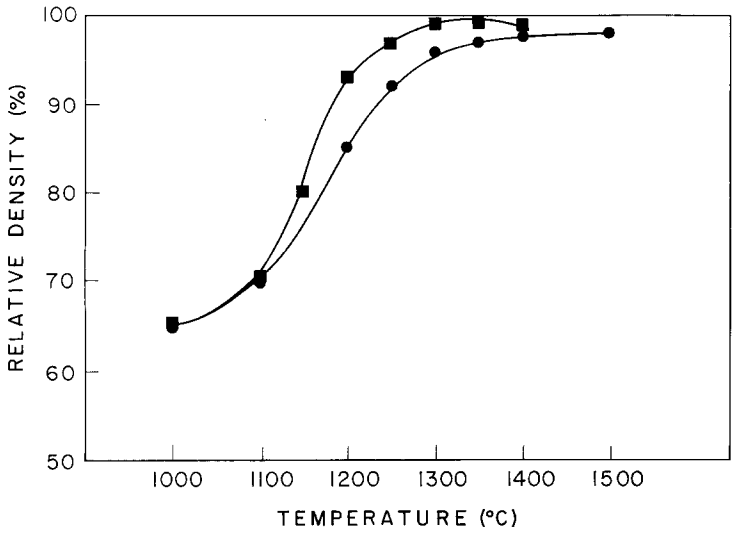

Figure 3 The effect of the vol% zirconia on the end-point density of magnesia–zirconia composites: (■) 20% ZrO_2 (DK1) + 2% MnO; (●) 40% ZrO_2 (DK1) + 2% MnO.

undoped samples. Additions of FeO also led to enhanced densification compared to the undoped samples. However, MnO was found to be a more effective densification aid than FeO. With 2 mol % MnO, calculated on the basis of MgO, density in excess of 97% at 1250° C and in excess of 99% at 1300° C could be achieved. Fig. 2b shows the effect of the concentration of MnO on sintering behavior. As shown in the figure, higher densities are achieved with 2 mol % MnO addition than with 3 mol % MnO. Finally, Fig. 3 shows the effect of the volume fraction of zirconia on the end-point density. As seen in the figure, samples containing 20 vol % zirconia achieve higher density compared to samples containing 40 vol % zirconia under similar sintering conditions. For most of the work, the samples made either by isostatic pressing or by slip casting were in the form of bars or plates. However, some crucibles were fabricated by slip casting in order to demonstrate the feasibility of fabricating complex-shaped parts. Fig. 4 shows a photograph of a slip cast and sintered crucible containing 20 vol % ZrO_2–80 vol % MgO.

In order to reveal the microstructural details, a two-step thermal etching process was employed. In the first step, thermal etching was done at 1420° C (for 15 min), which is the same as the sintering temperature, to reveal grain boundaries between similar phases. In the second step, the samples were thermally etched at 930° C for 30 min to reveal the fine structure within the zirconia grains. Scanning electron micrographs of a sample containing 40 vol % ZrO_2–60 vol % MgO at two magnifications are shown in Figs 5a and b. As seen in Fig. 5a, the grain sizes of both the zirconia- and magnesia-rich phases are of the order of 1.4 μm and that zirconia is well dispersed in the magnesia matrix. A higher magnification micrograph of the same sample in Fig. 5b shows very fine, uniform-sized domains within the zirconia grains. The domain structure was observed throughout the zirconia region. The domain size is of the order of 240 nm. Some of the samples were annealed at 1600° C for 110 h in order to cause grain growth. Scanning electron micrographs of the annealed samples after the two-step thermal etching procedure, are shown in Figs 5c and d. As seen in Fig. 5c, annealing at 1600° C led to an enhancement of the grain sizes of both of the phases. The grain sizes of both of the phases are of the order of 6.5 μm. However, as shown in Fig. 5d, the size of the domains within the zirconia grains was unchanged by the annealing treatment.

Fig. 5e shows a micrograph of a sample containing 40 vol % ZrO_2–60 vol % MgO in which 8 mol % CaO, on the basis of zirconia, was added. This sample was also thermally etched using the two-step process described previously. As seen in the micrograph, the grain sizes of the zirconia- and magnesia-rich phases are essentially the same as those in the samples devoid of calcia. However, a higher magnification micrograph of the zirconia-rich regions given in Fig. 5f shows that there are no domains in the samples containing CaO.

TABLE I Volume per cent of zirconia(ss) determined by systematic point-counting procedure

ZrO_2 added (vol %)	Measured zirconia(ss) (vol %)
10	12.8
20	22.8
30	32.0
40	43.4
50	54.4
60	65.0

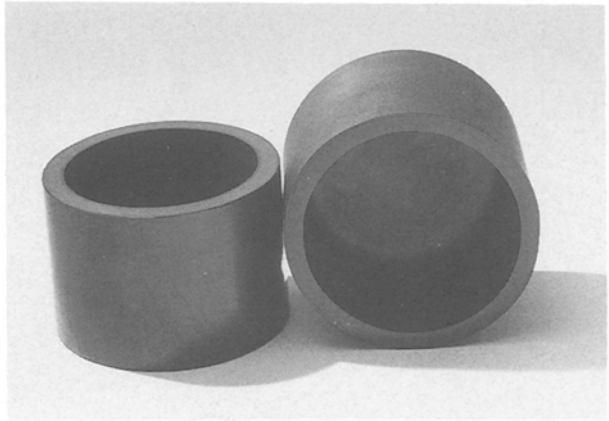

Figure 4 A photograph of a slip-cast and sintered MgO + 20 vol % ZrO_2 crucible.

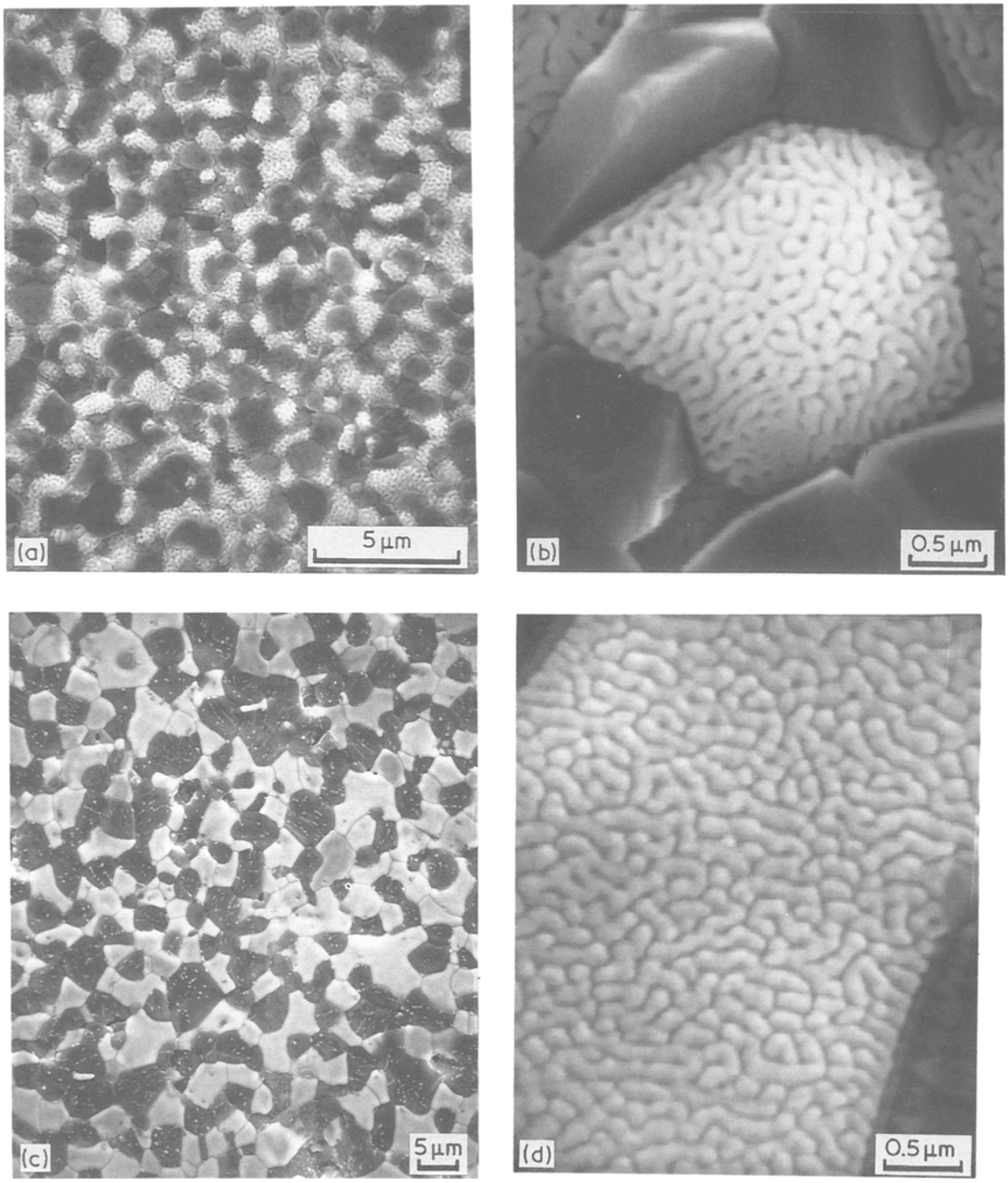

Figure 5 (a) A scanning electron micrograph of a sintered sample containing 40 vol % ZrO_2. Magnesia-rich phase appears dark while the zirconia-rich phase is light. The average grain size of both of the phases is $\sim 1.4\,\mu m$. (b) A higher magnification scanning electron micrograph of the sample in (a) showing the existence of very fine (240 nm), uniform-sized domains within the zirconia grains. (c) A scanning electron micrograph of a sample containing 40 vol % ZrO_2 that was annealed at 1600° C for 110 h. The annealing treatment led to an increase in the grain sizes of both of the phases. Average grain size $\sim 6.5\,\mu m$. (d) A higher magnification scanning electron micrograph of a zirconia grain from sample shown in (c). The zirconia grain in this sample also consists of very fine, uniform-sized domains. Note that the domain size is identical in (b) and (d). (e) A scanning electron micrograph of a calcia-doped (8 mol % CaO) sample containing 40 vol % ZrO_2. The average grain size is of the order of $1.4\,\mu m$. (f) A higher magnification scanning electron micrograph of zirconia grain from sample in (e). Note the lack of domain structure in zirconia.

3.2. Mechanical characterization

Mechanical characterization involved the measurement of strength and toughness. Fig. 6 shows a plot of strength of slip-cast secimens, measured at room temperature, as a function of volume fraction of zirconia. The data for pure magnesia was obtained on hot-pressed samples. As seen in the figure, strength increases with increasing volume fraction of zirconia. For samples containing 40 vol % ZrO_2, strength was as high as 480 MPa. By contrast, the strength of fine-grained MgO is only about 200 MPa. Two sets of samples containing 40 vol % ZrO_2 were fabricated by isostatic pressing followed by pressureless sintering; one set containing 8 mol % CaO while the other

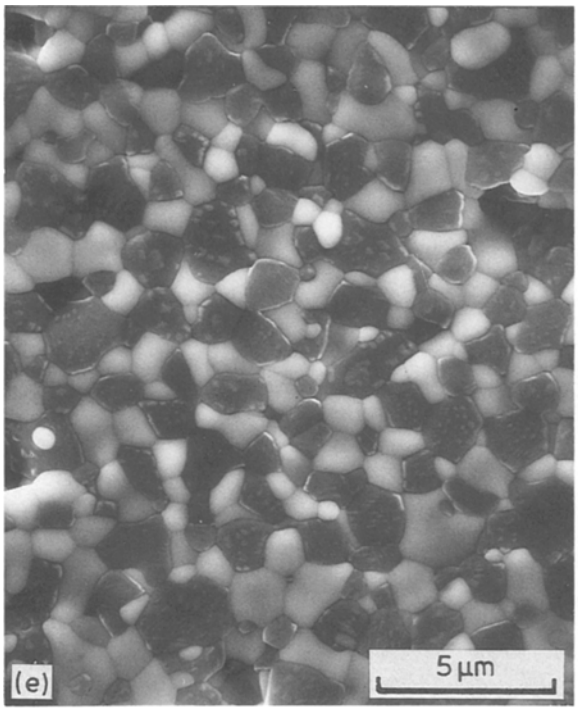

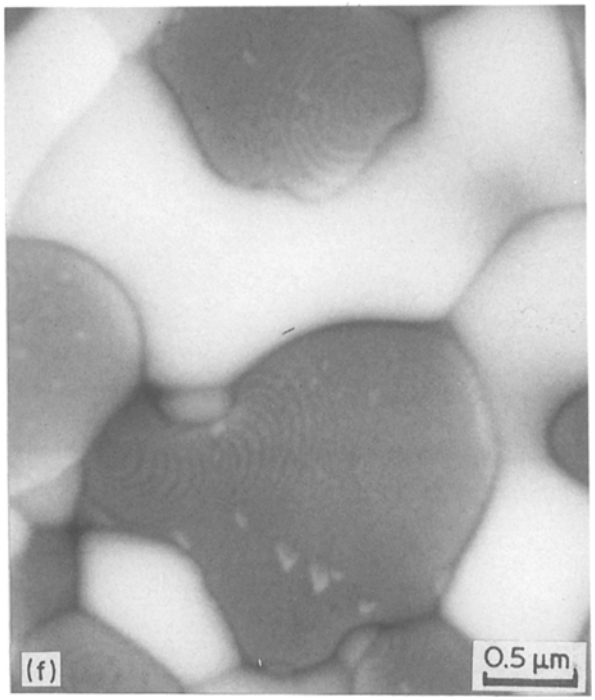

Figure 5 Continued.

contained no CaO. Room-temperature fracture strength of calcia-doped samples was 300 MPa and that of samples without calcia was 506 MPa.

Fracture strength of slip-cast samples containing 20 and 40 vol % zirconia was also measured as a function of temperature up to 1000° C. These data are shown in Fig. 7. As shown in the figure, the strength is essentially independent of temperature over the range of temperatures tested and the samples fractured in a brittle manner. Actually, the data exhibit a slight increase in strength, although this may not be significant. For this set of samples, strength in excess of 400 MPa for samples containing 40 vol % ZrO_2 is observed.

Fracture toughness of samples containing 40 vol % ZrO_2–60 vol % MgO was measured at room temperature and at 1000° C using single-edge notched beam in bending. The K_c was measured as 5.2 MPa $m^{1/2}$ at room temperature and 5.7 MPa $m^{1/2}$ at 1000° C. By contrast, the K_c of samples containing 8 mol % calcia was only 3.0 MPa $m^{1/2}$ and that of hot-pressed pure magnesia was about 1.8 MPa $m^{1/2}$.

3.3. X-ray diffraction and fractography

X-ray diffraction traces obtained with Cu$K\alpha$ radiation on MgO–ZrO_2 samples (without calcia) in the as-sintered condition exhibited the presence of two phases: magnesia and zirconia. On the basis of X-ray diffraction patterns, the zirconia-rich phase appeared to be cubic. However, as discussed previously, thermal etching revealed the presence of fine structure inside the grains of zirconia, the significance of which will be discussed in Section 4. X-ray diffraction traces from the as-sintered, ground and fracture surfaces failed to reveal the presence of any monoclinic phase. X-ray diffraction traces of calcia-doped samples also showed two phases: magnesia and cubic zirconia. No monoclinic phase was observed on as-sintered, ground and fracture surfaces.

An examination of fracture surfaces under an optical microscope and a scanning electron microscope showed that processing defects such as agglomerates and voids were generally the fracture initiation sites. A typical SEM fractograph is shown in Fig. 8.

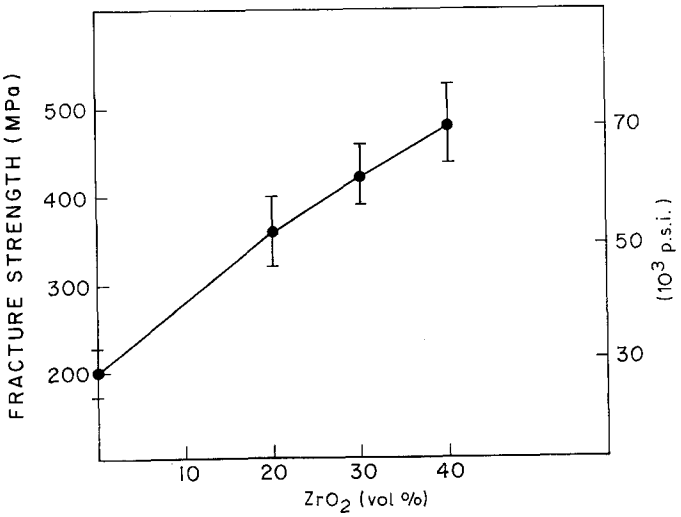

Figure 6 Strength plotted against vol % ZrO_2 of slip-cast, pressureless sintered MgO–ZrO_2 ceramics: 2% MnO, sintered 1400° C, 2 h.

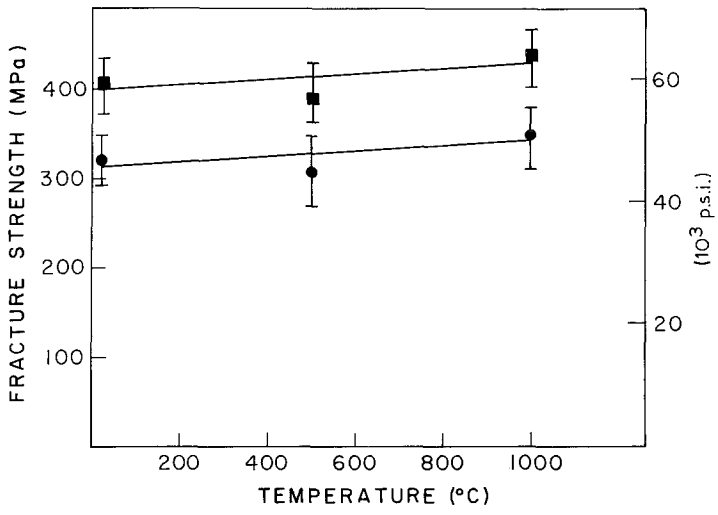

Figure 7 Fracture strength of pressureless sintered (●) MgO + 20 vol % ZrO_2 and (■) MgO + 40 vol % ZrO_2 ceramics as a function of temperature: sintered 1400° C, 2 h.

4. Discussion

4.1. Sintering

Fig. 1 shows that MgO–20 vol % ZrO_2 specimens sinter to a greater density compared to pure MgO above ~ 1200° C. This observation can be rationalized on the basis of point defects in MgO, which is the matrix material. Nelson and Cutler [17] examined the effect of various additives on sintering of MgO. They observed that the end point densities were greater in samples doped with TiO_2 and ZrO_2. The results were rationalized on the basis of cation vacancy formation [18]. The enhanced densification observed in the present work in two-phase magnesia–zirconia ceramics may be explained on the following premises.

(1) Some amount of ZrO_2 dissolves in MgO [19] thereby enhancing the cation vacancy concentration. For example, the incorporation of ZrO_2 in MgO may occur as follows

$$ZrO_2 \rightarrow Zr_{Mg}^{\cdot\cdot} + 2O_O^x + V_{Mg}'' \qquad (1)$$

(2) The presence of excess ZrO_2 serves to pin the grain boundaries thereby allowing the pores to remain at grain boundaries and promote densification.

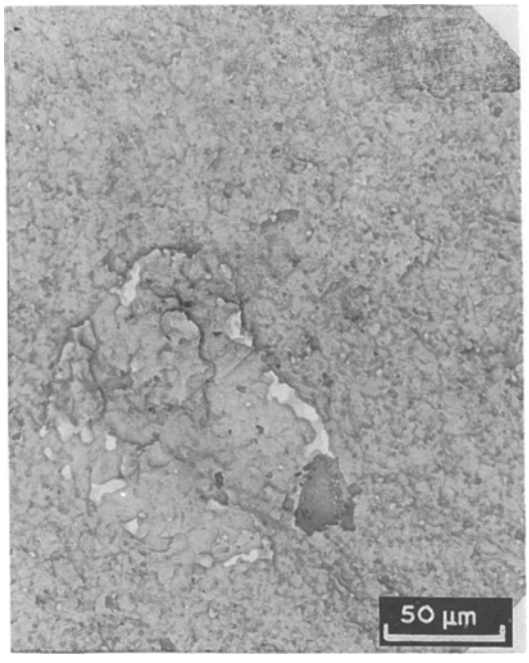

Figure 8 An SEM fractograph of an MgO + 20 vol % ZrO_2 sample showing the failure origin.

The effect of MnO as a sintering aid is shown in Fig. 2a. As shown in the figure, addition of MnO facilitates the densification of MgO–20 vol % ZrO_2 ceramics. Additions of FeO were similarly found to be beneficial in enhancing the end-point densities. This effect can also be rationalized on the basis of defect chemistry. In the actual experiments, manganese and iron were added as divalent compounds, MnO and FeO, respectively. However, at elevated temperatures where rapid equilibration occurs, manganese and iron are expected to assume various valences. For example, in the case of manganese, the valence states expected are +2, +3 and +4. In the case of iron, the valence states expected are +2 and +3. If the relevant thermodynamic data are available, the relative concentrations of the various species can, in principle, be determined. For example, Mason and Bowen [20] have examined cation valencies in Fe_3O_4. It is not the objective of the present work to examine defect reactions and defect equilibria in doped MgO. However, if for the sake of illustration it can be assumed that the dopant predominantly exists in the +3 state, the following defect reaction is plausible

$$MnO/FeO + \tfrac{1}{4}O_2(g) \rightarrow Mn_{Mg}^{\cdot}/Fe_{Mg}^{\cdot} + \tfrac{3}{2}O_O^x + \tfrac{1}{2}V_{Mg}'' \qquad (2)$$

Thus, the cation vacancy concentration is proportional to the dopant concentration. If cation transport predominantly occurs by the movement of vacancies and if the cations are the slower moving species, addition of MnO or FeO (in which the cations are incorporated in the trivalent state) is expected to enhance the sintering kinetics, as observed. MnO dissolves in MgO to a significant extent. If the concentration of the dopant is increased beyond a certain limit, the vacancy concentration on the anion sublattice will be so suppressed that oxygen transport may become rate limiting. Further increase in the dopant concentration then is expected to suppress the kinetics of sintering. Indeed this has been observed as shown in Fig. 2b which shows that samples doped with 2 mol % MnO sinter to a higher density compared to the samples doped with 3 mol % MnO. For maximizing the sintering

kinetics, it is essential to examine a range of dopant concentrations. This, however, was not done in the present work. It is possible that the maximum sintering kinetics and end-point densities may be achieved at a concentration of the dopant different from that used in the present work.

Fig. 3 shows that MgO–20 vol % ZrO_2 specimens sinter to a higher density at a given temperature in comparison to MgO–40 vol % ZrO_2 specimens. This is not surprising because MgO sinters at a lower temperature compared to ZrO_2. Thus, specimens containing smaller amount of ZrO_2 (but greater than the solubility limit) sinter more easily. At low volume fractions of the zirconia phase, the sintering behaviour of the two-phase materials seems to be influenced by the kinetics of sintering of the magnesia-rich phase. Thus, enhancement of sintering kinetics of the matrix phase has a beneficial effect on the sinterability of the two-phase material. Decrease of sintering rate with increasing zirconia-rich phase indicates that zirconia is more difficult to sinter.

4.2. Microstructure and phases

According to the phase diagram [12–14], above about 1400° C, the two phases in coexistence are magnesia(ss) and cubic zirconia(ss). The eutectoid temperature and composition are ~1400° C and 13.5 mol % ZrO_2, respectively. Conceivably, samples cooled rapidly from the sintering temperature ($\geqslant$1400° C) should retain the high-temperature cubic zirconia phase to room temperature. X-ray diffraction of the as-sintered, ground and fracture surfaces exhibited the presence of magnesia and zirconia (apparently cubic) phases. On the basis of X-ray diffraction patterns, the zirconia-rich phase appears to be of the cubic polymorph; specifically, no split between (4 0 0) and (0 0 4) peaks was observed. The scanning electron micrograph given in Fig. 5a shows that the microstructure is fine-grained with grain sizes of the magnesia-rich and zirconia-rich phases of the order of 1.4 μm. However, after thermal etching at 930° C for 30 min, zirconia grains showed very fine substructure as shown in Figs 5b and d. The substructure resembles an assemblage of tiny (~240 nm), uniform-sized domains. Such substructure is not expected in the cubic phase.

Recent work [21–24] has shown that certain ordered phases form in rapidly cooled samples in the MgO–ZrO_2 system. For example, the ordered phase of the stoichiometry $Mg_2Zr_5O_{12}$ (δ-phase) is known to form under certain circumstances. In samples containing 20.8 mol % MgO and 79.2 mol % ZrO_2, Sim and Stubican [24] showed evidence of the δ-phase in samples quenched from 2035° C and annealed at 800° C for 40 d. This clearly suggests that the δ-phase forms by some diffusional process which it must, because the initial composition of their alloy was 20.8 mol % MgO while the δ-phase contains 28.5 mol % MgO. In their samples sintered at 1600° C and quenched to room temperature, only the cubic solid solution was observed by the authors [24]. In the present experiments, the samples were thermally etched for only 30 min at 930° C. Diffusional processes at such a low temperature are so slow that little diffusion is expected in such a short time. Thus, the composition of the zirconia-rich phase (and for that matter of the magnesia-rich phase) is not expected to change during the relatively short thermal etching procedure. The formation of the domain structure must therefore have occurred earlier, and thus the samples in the present work did not contain the $Mg_2Zr_5O_{12}$ phase. Recent work by Readey *et al.* [25] has shown that the (1 1 1) peak exhibits a shoulder on the high-angle side if the ordered δ-phase is present. No such shoulder was observed in the present work. Thermal etching at 930° C simply reveals the already present domain structure. This is further verified by X-ray diffraction traces taken from thermally etched samples which show an identical pattern to that from as-sintered samples.

In order to elucidate the nature of the domain structure and its origins, some of the samples were sintered at ~1325° C, which is below the eutectoid decomposition temperature. That is, the samples were sintered in the two-phase field containing tetragonal zirconia(ss) and magnesia(ss). No domain structure was observed in these samples after thermal etching at 930° C. Also, the samples exhibited profuse cracking in the as-sintered state associated with the spontaneous tetragonal → monoclinic transition. X-ray diffraction confirmed the presence of the monoclinic phase in these materials. These results indicate that the domain structure is somehow related to sintering in the stability range of cubic zirconia(ss) followed by cooling to lower temperatures.

As discussed in the following, the origin of domain-type structure observed in the present work appears to be related to the nature of cubic → tetragonal transformation in zirconia. Scott [26] studied phase transformations in the Y_2O_3–ZrO_2 system. He showed that a diffusionless transition from cubic → tetragonal occurs in certain alloys leading to the development of a multiply twinned microstructure. This transition subsequently was studied by Michel *et al.* [27], Sakuma [28] and more extensively by Heuer *et al.* [29]. The displacively formed tetragonal phase is referred to as the t′-phase. The morphology of the t′-phase resembles domains or twins. Heuer *et al.* [29] have shown that the domains or the twins exist in three orthogonal (nearly) orientation sites. (The domains or the twins were further shown to contain ordered domains of ~20 to 100 nm size characterized by the existence of anti-phase boundaries [28, 29].) The reason for the formation of the twin-type structure with three orthogonal (nearly) variants is the minimization of the strain energy. The low-temperature tetragonal polymorph of zirconia is known to be ferroelastic [27, 30] and the cubic → tetragonal composition invariant transformation is of the paraelastic → ferroelastic displacive type. Thus, the so-called t′-phase is a ferroelastically formed phase.

The presence of the three orthogonal variants in yttria-doped zirconia can also be confirmed on the basis of electron diffraction pattern with ⟨1 0 0⟩ type of zone axis in which spot splitting is observed [31]. As-fired samples of zirconia containing ~10 mol %

MgO in Hannink's work [32] also gave an electron diffraction pattern which is consistent with the presence of three orthogonal variants. Samples in Hannink's work were sintered in the stability range of the cubic phase. In the present work also the samples were sintered in the stability range of the cubic phase field. The fine substructure observed in the zirconia-rich regions in $MgO–ZrO_2$ samples sintered at $\geqslant 1400°$ C in the present study appears to be due to the displacively, ferroelastically formed tetragonal zirconia. That is, the apparent cubic phase observed at room temperature must be of tetragonal symmetry but with a c/a ratio too close to unity to be discernible by conventional X-ray diffraction. It is well known that the c/a ratio decreases with increasing amount of the stabilizer. Because the domains are expected to occur in three (orthogonal) orientations, it is expected that domain boundaries would exhibit thermal grooving. Thus, the domain structure is revealed by thermal etching.

If the entire cubic grain of zirconia converts into a tetragonal grain, substantial distortion of the surrounding matrix must occur which would involve absorption of elastic energy which is approximately proportional to the size of the crystal. However, if the crystal converts into a polydomain structure such that the tetragonal domains are oriented with [0 0 1] directions in three mutually orthogonal directions, the strain energy is minimized The smaller the domain size, the lower will be the total strain energy. The strain energy is minimized. The smaller the domain the domain size should be as small as possible. However, the interfaces between the domains would have some interfacial energy. Clearly, the size of the domains will be dictated by the minimization of the sum of the strain and the interfacial energies. Khachaturyan [33] has examined the problem of domain size in cases where there are effectively two orientation states (the so-called 180° domains). Actually, Khachaturyan has examined the case of one-dimensional compositional modulation, which turns out to be analogous to 180° domains. The domains observed in the zirconia-rich phase are believed to be due to the cubic → tetragonal displacive transformation and are the so-called 90° domains. According to Khachaturyan, for a polydomain cyrstal in the shape of a paralleliped of square cross-section of dimension S and of length L, the domain size δ is given by

$$\delta \approx \left(\frac{\gamma_s S}{4\lambda\varepsilon^2}\right)^{1/2} \tag{3}$$

where λ is the pertinent elastic modulus, ε is the strain mismatch and γ_s is the interfacial energy. In terms of the measured domain size, the interfacial energy may be given by

$$\gamma_s \approx \frac{4\lambda\varepsilon^2\delta^2}{S} \tag{4}$$

The experimental value of δ is of the order of 240 nm. Assuming the modulus to be 250 GPa, measured grain size S as 1.4 μm and assuming the c/a ratio of tetragonal zirconia to be 1.003 (so that ε is of the order of 0.003), the calculated value of γ_s is of the order of 0.37 J m^{-2}. As many approximations are made in the above calculation, the value of the interfacial energy is not expected to be very accurate. However, the calculated value, which represents inter-domain boundary energy appears to be reasonable as the inter-domain boundaries are expected to be fully or partially coherent.

Equation 3 shows that the domain size is proportional to the square root of the precipitate or the grain size. However, it was observed in the present work that the domain size was independent of the grain size (see Figs 5b and d). This discrepancy may be related to the fact that Khachaturyan's [33] calculation assumes a paralleliped-shaped particle in an infinite matrix. In the present case, however, the volume fraction of zirconia is about 0.45 and that zirconia grains are uniformly dispersed. Khachaturyan's [33] calculation would suggest that as the volume of the particle increases, so does the domain size. In our preliminary work we have determined the domain size as a function of volume fraction of zirconia. It was observed that the domain size in a sample containing ~ 6 vol % zirconia was about twice that in a sample containing ~ 10 vol % zirconia. The other source of the discrepancy relates to the fact that Khachaturyan's [33] calculation is for a one-dimensional case while the domains in the present material are expected to be oriented in three, mutually orthogonal directions [29, 31].

The microstructure of samples containing CaO was identical with regards to the grain sizes of the two phases as shown in Figs 5a and e. Chemical analysis using energy dispersive analysis of X-rays (EDAX) also showed that the concentration of MgO in the zirconia-rich phase was about the same. However, thermal etching of samples containing CaO did not reveal domain substructure as shown in Fig. 5e. X-ray diffraction indicated that the zirconia-rich phase did not exhibit (4 0 0)/(0 0 4) split and the peak was symmetrical. Based on this information, it is concluded that some of the calcia that dissolved in zirconia must have stabilized the cubic phase of zirconia to room temperature.

4.3. Strength and fracture toughness

Fig. 6 shows that the strength of $MgO–ZrO_2$ specimens increases with increasing amount of the zirconia-rich phase. Strength of the order of 500 MPa can be realized in compositions containing 40 vol % ZrO_2. By contrast, fine-grained, hot-pressed MgO exhibited strength of only 200 MPa. This shows the beneficial effect of zirconia phase on the strength of $MgO–ZrO_2$ ceramics. As pointed out earlier, no transformation to the monoclinic phase was observed. The increase in strength may possibly be attributed to dispersion strengthening by mechanisms such as crack deflection. However, addition of CaO led to a significant lowering of strength and toughness. For example, the strength and toughness of samples containing 40 vol % ZrO_2 were 506 MPa and 5.2 MPa m$^{1/2}$, respectively. By contrast, samples of the same composition and essentially identical microstructure but doped with 8 mol % CaO exhibited a strength of only 300 MPa and a toughness of 3.0 MPa m$^{1/2}$. Fracture topography in undoped and calcia-doped samples was essentially identical. This

suggests that calcia doping is not expected to affect the degree of crack deflection. Hence, the enhanced strength and toughness of samples without calcia cannot be explained based on crack deflection alone.

As discussed previously, zirconia phase in the calcia-doped samples is cubic while that in the undoped samples must be tetragonal. It is tempting to attribute the higher strength and toughness of undoped samples to transformation toughening. However, no monoclinic phase was observed on as-sintered, ground or fracture surfaces. It may be argued, as has been done for other zirconia-based materials [34, 35], that reverse transformation to the tetragonal phase may have occurred once the crack has passed through. The zirconia phase in the present study contained a very high amount of dissolved MgO (~ 13.5 mol %). With such a high supersaturation, the t $\rightarrow$ m transition temperature is expected to be substantially depressed, even possibly to room temperature or below. Thus, any possible transformation toughening effect, inclusive of reverse transformation, is not expected to be operative at temperatures much above room temperature. Fig. 7, however, shows that the strength of samples containing 20 and 40 vol % ZrO_2 is independent of temperature up to 1000° C, the maximum test temperature employed in the present work. It may thus be concluded that the toughening effect in the present materials is not related to transformation toughening.

It has been shown that tetragonal zirconia is a ferroelastic material [27, 30]. Virkar and Matsumoto [30] proposed ferroelastic domain switching as a toughening mechanism in polycrystalline tetragonal zirconia. However, no evidence of domain switching on fracture surfaces was presented. Recently, Srinivasan *et al.* [31] observed domain switching on fracture surfaces of yttria-stabilized polydomain single crystals. These crystals also exhibited high toughness at 1000° C similar to the observations of Ingel *et al.* [36]. These results suggest that toughening effect in the present materials may be due to ferroelastic domain switching. However, no evidence of domain switching could be obtained as the c/a ratio is too small to distinguish the (4 0 0) and (0 0 4) peaks. Currently, experiments are underway using transmission electron microscopy to determine the degree of tetragonality.

The most interesting aspect of the present results is the invariance of the strength and the toughness with temperature. As mentioned earlier, in samples containing 20 and 40 vol % ZrO_2, the strength and toughness was found to be independent of temperature up to 1000° C, the maximum test temperature employed in the present work. Thus, the present work shows that moderately high strength and toughness at elevated temperatures can be realized in zirconia-containing ceramics. Further, the present work also shows that magnesia can be toughened by the incorporation of zirconia.

Acknowledgement

This work was supported by Dow Chemical Company, Midland, Michigan.

References

1. R. C. GARVIE, R. H. J. HANNINK and R. T. PASCOE, *Nature (London)* **258** (1975) 703.
2. D. L. PORTER and A. H. HEUER, *J. Amer. Ceram. Soc.* **62** (1979) 298.
3. R. R. HUGHAN and R. H. J. HANNINK, *ibid.* **69** (1986) 556.
4. R. H. J. HANNINK and R. C. GARVIE, *J. Mater. Sci.* **17** (1982) 2637.
5. M. V. SWAIN, *Acta Metall.* **33** (1985) 2083.
6. P. F. BECHER and M. K. FERBER, *J. Mater. Sci.* **12** (1987) 973.
7. A. H. HEUER, *J. Amer. Ceram. Soc.* **70** (1987) 689.
8. N. CLAUSSEN, *ibid.* **59** (1976) 49.
9. N. CLAUSSEN and J. JAHN, *ibid.* **63** (1980) 228.
10. L. VISWANATHAN, Y. IKUMA and A. V. VIRKAR, *J. Mater. Sci.* **18** (1983) 109.
11. N. CLAUSSEN and J. JAHN, *J. Amer. Ceram. Soc.* **61** (1978) 94.
12. P. DUWEZ, F. ODELL and F. H. BROWN Jr, *ibid.* **35** (1952) 107.
13. D. VIECHNICKI and V. S. STUBICAN, *ibid.* **48** (1965) 292.
14. C. F. GRAIN, *ibid.* **50** (1967) 288.
15. Y. IKUMA, W. KOMATSU and S. YAEGASHI, *J. Mater. Sci. Lett.* **4** (1985) 63.
16. P. BASCOM, Senior Thesis, University of Utah, (1985).
17. J. W. NELSON and I. B. CUTLER, *J. Amer. Ceram. Soc.* **41** (1958) 406.
18. J. T. JONES, P. K. MAITRA and I. B. CUTLER, *ibid.* **41** (1958) 353.
19. T. S. IGNATOVA, L. V. UZBERG, V. A. PEREPELITSYN and G. V. GAUER, *Neorg. Mater.* **9** (1973) 805.
20. T. O. MASON and H. K. BOWEN, *J. Amer. Ceram. Soc.* **64** (1981) 86.
21. C. DELAMARRE, *C. R. Hebd. Seances Acad. Sci. Ser C* **269** (1965) 113.
22. H. J. ROSSELL and R. H. J. HANNINK, "The $Mg_2Zr_5O_{12}$ Alloy in MgO Partially Stabilized Zirconia", in "Advances in Ceramics, Science and Technology of Zirconia", Vol. 12, edited by N. Claussen, M. Rühle and A. H. Heuer (American Ceramic Society, Columbus, Ohio, 1984) pp. 139–51.
23. S. C. FARMER, L. H. SCHOENLEIN and A. H. HEUER, *J. Amer. Ceram. Soc.* **66** (1983) 107.
24. S. M. SIM and V. S. STUBICAN, *ibid.* **70** (1987) 521.
25. M. J. READEY, A. H. HEUER and R. W. STEINBRECH, *ibid.* **71** (1988) C-2.
26. H. G. SCOTT, *J. Mater. Sci.* **10** (1975) 1527.
27. D. MICHEL, L. MAZEROLLES and M. PEREZ Y JORBA, *ibid.* **18** (1983) 2618.
28. T. SAKUMA, *ibid.* **22** (1987) 4470.
29. A. H. HEUER, R. SCHAIM and V. LANTERI, *Acta Metall.* **35** (1987) 661.
30. A. V. VIRKAR and R. L. K. MATSUMOTO, *J. Amer. Ceram. Soc.* **69** (1986) C-224.
31. G. V. SRINIVASAN, J. F. JUE, S. Y. KUO and A. V. VIRKAR, *ibid.* (1988) submitted.
32. R. H. J. HANNINK, *J. Mater. Sci.* **13** (1978) 2487.
33. A. G. KHACHATURYAN, "Theory of Structural Transformations" (Wiley, New York, 1983).
34. D. B. MARSHALL and M. R. JAMES, *J. Amer. Ceram. Soc.* **69** (1986) 215.
35. B-S LI, J-S CHERNG, K. J. BOWMAN and I-W CHEN, *ibid.* **71** (1988) C-362.
36. R. P. INGEL, D. LEWIS, B. A. BENDER and R. W. RICE, *ibid.* **65** (1982) C-150.

Received 22 August 1988
and accepted 11 January 1989